

## Article

# Crosslinked PVA/Citric Acid Nanofibrous Separators with Enhanced Mechanical and Thermal Properties for Lithium-Ion Batteries

Shuangyang Cai, Yuexi Liang, Jialu Wu, Haizhen Chen, Zhenzhen Wei \*<sup>ID</sup> and Yan Zhao \*<sup>ID</sup>

National Engineering Laboratory for Modern Silk, College of Textile and Clothing Engineering, Soochow University, Suzhou 215123, China; 20215215104@stu.suda.edu.cn (S.C.); 2115405016@stu.suda.edu.cn (Y.L.); 2115404009@stu.suda.edu.cn (J.W.); 20215215052@stu.suda.edu.cn (H.C.)  
\* Correspondence: zzwei@suda.edu.cn (Z.W.); yanzhao@suda.edu.cn (Y.Z.)

**Abstract:** Electrospinning polyvinyl alcohol (PVA) nanofibrous membranes have gained increased attention for their uses as separators for lithium-ion batteries (LIBs) due to their high porosity and excellent electrolyte wettability, but their poor mechanical and thermal properties have limited their further development. In this work, a crosslinked PVA composite separator (PVA/CA-H) was first prepared via the electrospinning of the PVA and citric acid (CA) mixed solution and then the heating of the nanofibrous membrane, and the effects of the amount of CA on the structure and performance of the PVA/CA-H separator were investigated. The hydroxyl group of PVA and the carboxyl group of CA were crosslinked under the heat treatment, resulting in a slight reduction in the porosity and pore size of the composite separator compared to pure PVA, and to compensate for this issue, the mechanical strengths, as well as the thermal dimensional stability of the PVA/CA-H separator, were significantly improved. Meanwhile, the PVA/CA-H separator exhibited good electrolyte uptake (158.1%) and high ionic conductivity ( $1.63 \text{ mS cm}^{-1}$ ), and, thus, the battery assembled with the PVA/CA-H separator exhibited a capacity retention of 96.3% after 150 cycles at 1 C. These features mean that the crosslinked PVA composite separator can be considered as a prospective high-safety and high-performance separator for LIBs.



**Citation:** Cai, S.; Liang, Y.; Wu, J.; Chen, H.; Wei, Z.; Zhao, Y. Crosslinked PVA/Citric Acid Nanofibrous Separators with Enhanced Mechanical and Thermal Properties for Lithium-Ion Batteries. *Batteries* **2023**, *9*, 556. <https://doi.org/10.3390/batteries9110556>

Academic Editor: Claudio Gerbaldi  
Received: 23 October 2023  
Revised: 9 November 2023  
Accepted: 13 November 2023  
Published: 15 November 2023



**Copyright:** © 2023 by the authors. Licensee MDPI, Basel, Switzerland. This article is an open access article distributed under the terms and conditions of the Creative Commons Attribution (CC BY) license (<https://creativecommons.org/licenses/by/4.0/>).

## 1. Introduction

Lithium-ion batteries (LIBs) play a pivotal role in the development of new energy and environmental protection, as well as other major technological fields, due to their excellent performance, such as low cost, high energy density, high power, prolonged service life, etc. [1]. The separator, a crucial component of the LIB, serves as a channel for lithium-ion migration between the electrodes, in addition to its function in physically separating the positive and negative electrodes [2]. The internal resistance and interfacial structure of battery are directly influenced by the separator's performance, which also has an impact on other aspects of cells, such as discharge capacity, cycling efficiency, and safety. Therefore, an ideal separator is required to have uniform pore distribution, high porosity, good electrolyte wettability, robust mechanical strength, and great thermal stability.

Currently, microporous polyolefin separators, primarily referring to polypropylene (PP) and polyethylene (PE) separators, are considered to be the most popular separators utilized in LIBs due to their good chemical stability, desirable mechanical strength, and low cost. However, these polyolefin separators present poor thermal stability owing to their inherent low melting point (i.e.,  $\leq 165^\circ\text{C}$ ) [3]. More importantly, they cannot effectively meet the requirements of the rapid charging and discharging of high-power batteries because of their low porosity and poor electrolyte wettability, and, thus, the safety and cycle life of the batteries are affected. Many efforts have been made to address these issues

affecting polyolefin separators, such as grafting polar functional groups [4,5] and coating organic polymers [6,7] and inorganic particles [8,9] on the surface, thereby improving their electrolyte wettability and thermal stability. In addition to the surface modification based on polyolefin separators, a variety of novel materials, such as polyvinylidene fluoride (PVDF) [10,11], polyacrylonitrile (PAN) [12,13], polyimide (PI) [14,15], or cellulose [16,17], have been built into separators via different methods, including electrospinning, phase separation, vacuum filtration, freeze-drying, etc. [18]. Many of these separators displayed excellent overall performance and have the potential to be polyolefin's substitutes.

Polyvinyl alcohol (PVA), one of representative polymers, has also been selected as the original material for the separator's fabrication. Due to its regular molecular structure with a large number of hydroxyl groups in the molecular chain, PVA exhibits excellent processability, electrolyte wettability, and chemical stability, all of which give it the opportunity to be applied in the field of separators. It has been reported that technologies including solution coating [19], non-solvent induced phase separation [20], and freeze-drying [21] have been applied to fabricate the PVA into composite separators, most of which present improved electrolyte affinity due to the rich hydroxyl group in PVA, thereby enhancing the electrochemical performance of the separator. Moreover, electrospinning is one of the most common techniques used to fabricate PVA separators, as it regulates pore homogeneity and affords the separator excellent porosity, which facilitates the transport of lithium ions at the electrode–electrolyte interface [22–24]. However, it is generally difficult for a nanofibrous separator to possess high porosity and robust mechanical strength at the same time, primarily because the nanofibrous membrane is composed of a 3D network interwoven by the nanoscaled fibers.

Crosslinking, one of the most common modification strategies, has the ability to link two or more molecules together via chemical bonds, and, thus, the crosslinked product not only shares the advantages of one specific molecule but also typically presents superior thermal and mechanical properties [25]. As PVA has multiple hydroxyl groups in its molecular chain structure and is easily crosslinked with various chemical groups, crosslinking PVA to prepare composite separators has also piqued the interest of researchers. For example, Fartash et al. [26] prepared PAN/PVA/MA separators via electrospinning, using malonic acid (MA) as a crosslinking agent with enhanced tensile strength and reduced thermal shrinkage. In another research, Gong et al. [27] fabricated the PVA/HNT composite separator via the electrospinning of PVA containing halloysite nanotubes (HNTs), followed by crosslinking via immersion in a glutaraldehyde dispersion. The PVA/HNT separator showed excellent thermal stability and mechanical properties due to the interlocking interconnections between the thermally resistant HNTs and the PVA matrix.

In this contribution, a crosslinked PVA composite nanofibrous separator for LIBs was prepared via electrospinning and the heat-induced crosslinking of PVA and citric acid (CA). CA is an organic acid containing carboxyl groups, which can be esterified with hydroxyl groups on the chain of PVA macromolecules under heating conditions [28]. Thus, it is reasonable to infer that crosslinking PVA with CA is a feasible strategy for property enhancement. Therefore, the morphology, chemical and porous structures, and mechanical, thermal and wettability properties, as well as the electrochemical and battery performances, of PVA composite separators with different CA contents were investigated. The obtained composite separator (PVA/CA-H) was capable of (i) possessing high porosity (68.9%) and good electrolyte uptake (158.1%); (ii) exhibiting excellent thermal properties and mechanical properties, increasing the tensile strength of PVA by 78.4% (from 7.4 MPa to 13.6 MPa); and (iii) demonstrating high ionic conductivity ( $1.63 \text{ mS cm}^{-1}$ ), which speeds up ion transport and significantly boosts the battery cycle performance. The remarkable properties of the PVA/CA-H composite separator show its potential in applications of LIBs for high safety and outstanding electrochemical performance.

## 2. Experimental

### 2.1. Materials

Polyvinyl alcohol (PVA, 1788), citric acid (CA), sodium hypophosphite (SHP), and *n*-butanol were supplied by Aladdin Reagent Co., Ltd. (Shanghai, China). Lithium metal (Li) anode and lithium iron phosphate (LiFePO<sub>4</sub>) cathode were provided by Shenzhen Kejing Technology Co., Ltd. (Shenzhen, China). Lithium hexafluorophosphate (LiPF<sub>6</sub>, 1 M) in ethylene carbonate, ethylmethyl carbonate, and dimethyl carbonate (EC/EMC/DMC, 1/1/1, *v/v/v*) was supplied by Ferro Corp (Mayfield Heights, OH, USA). All materials were ready for use without further purification.

### 2.2. Preparation of PVA/CA-H Nanofibrous Separator

As shown in Figure 1, the PVA/CA-H composite separator was prepared in the following manner. Firstly, the PVA/CA electrospun solution was prepared. Indeed, 0.8 g of PVA was dissolved in 9.2 mL deionized water, and certain amounts of CA and SHP (PVA:CA:SHP = 8:2:0.2, 8:4:0.4, 8:6:0.6, 8:8:0.8, *w/w/w*) were added and heated via stirring at 85 °C for 4 h to obtain the mixed PVA/CA solution. Secondly, the PVA/CA membrane was fabricated via the electrospinning of the mixed solution with a feed rate of 0.30~0.35 mL h<sup>-1</sup>, a high voltage of 24~26 kV, and a collector distance of 16 cm. According to the mass ratio of PVA to CA, these PVA/CA composite membranes were denoted as PVA/CA-2, PVA/CA-4, PVA/CA-6, and PVA/CA-8, respectively. Finally, the PVA/CA-H nanofibrous separator was obtained by treating these PVA/CA samples in the vacuum oven at 120 °C for 3 h and labeled as PVA/CA-H2, PVA/CA-H4, PVA/CA-H6, and PVA/CA-H8, respectively.

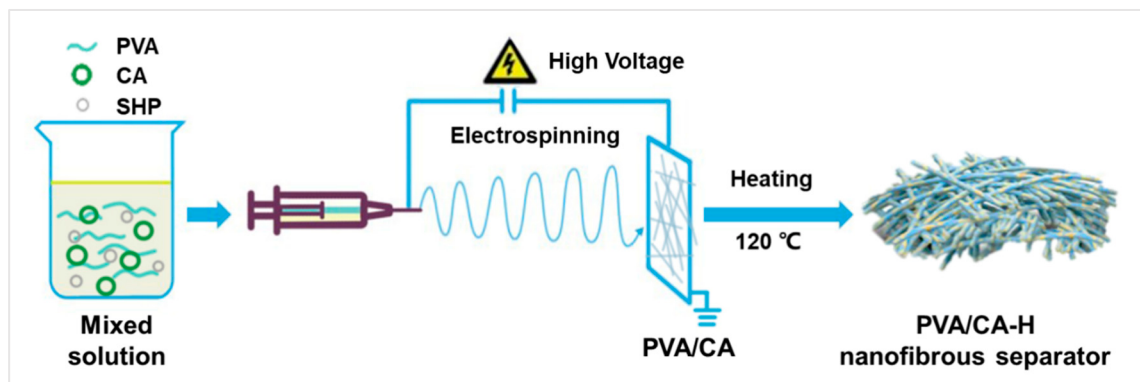


**Figure 1.** Schematic diagram for the preparation of the PVA/CA-H nanofibrous separator.

### 2.3. Characterization

The morphologies of PVA and its composite membranes were visualized using field emission scanning electron microscopy (FE-SEM, Hitachi S-4700, Hitachi, Tokyo, Japan). The chemical structure changes in PVA/CA before and after heating were examined via Fourier infrared spectroscopy (FT-IR, Nicolet 5700, Thermo Electron Co., Ltd., Waltham, MA, USA) in the range of 450 to 8000 cm<sup>-1</sup> at room temperature. The nanofibrous membranes' pore sizes were determined using a Porometer 3G through-hole size analyzer (CFP-1500a, Porous Materials, Inc., Ithaca, NY, USA) with a sample size of 5 cm × 5 cm. The porosity of the separator was obtained via the *n*-butanol absorption method. The separator was dipped into *n*-butanol for 2 h, and its porosity was determined using the following Equation (1):

$$\text{Porosity (\%)} = \frac{W_t - W_0}{\rho V} \times 100\% \quad (1)$$

where  $w_0$  and  $w_t$  stand for the separator's mass before and after *n*-butanol soaking, respectively;  $\rho$  represents the density of *n*-butanol (0.8098 g/cm<sup>3</sup>); and  $V$  is the volume of the sample separator.

The contact angle of the electrolyte (1 M LiPF<sub>6</sub>, EC/DEC/DMC 1:1:1) of the separator was measured using a contact angle analyzer (DSA100, Krüss GmbH, Hamburg, Germany). The electrolyte uptake (EU) was determined according to Equation (2) after immersion in the electrolyte for 2 h.

$$\text{EU (\%)} = \frac{W_b - W_a}{W_a} \times 100\% \quad (2)$$

where  $w_a$  and  $w_b$  represent the mass of the separator before and after absorbing the electrolyte, respectively.

The uniaxial tensile test was carried out on the samples using an Instron universal testing machine (Instron 5967, Instron Co., Ltd., Boston, MA, USA), with a clamping distance of 20 mm and a tensile speed of 20 mm/min. The puncture load of the separator was measured at a constant speed of 20 mm/min via the Instron universal testing machine equipped with a 2.5 mm diameter needle. Five specimens were measured for each sample, and the average value was taken. The thermal stability of the separators was tested using a thermogravimetric analyzer (TG, SDTQ600, Perkin Elmer, Waltham, MA, USA) with a heating rate of 10 °C/min under nitrogen from 30 °C to 700 °C. The separator's thermal dimensional stability was evaluated by measuring the dimensional change after around 1 h of heat treatment at 120 °C and 180 °C.

All the separators were tested for electrochemical properties by utilizing an electrochemical workstation (BioLogic SP-300, BioLogic Science Instruments, Seyssinet-Pariset, France). The assembly of all test cells (CR2025) was carried out in a glove box (high purity argon atmosphere) filled with 60 µL of electrolyte (LiPF<sub>6</sub>) solution and different electrodes. The separator's interfacial impedance was evaluated for interfacial compatibility profiling via electrochemical impedance spectroscopy (EIS) at an amplitude of 10 mV within a frequency range of 0.1 Hz to 0.1 MHz. The separator used for this measurement was sandwiched inside the LiFePO<sub>4</sub>/liquid-electrolyte-immersed separator/Li cell. Linear sweep voltammetry (LSV) was used to evaluate the separator's electrochemical stability via the assembly of the stainless steel (SS)/liquid-electrolyte-immersed separator/Li cell. And the LSV test was conducted at a scan rate of 5 mV s<sup>-1</sup> between 3.0 and 6.0 V versus Li/Li<sup>+</sup>. The separator's bulk impedance was measured via the assembly of the SS/liquid-electrolyte-immersed separator/SS cell and by utilizing EIS with an amplitude of 10 mV and a frequency range of 0.1–0.1 MHz. The ionic conductivity ( $\sigma$ ) was determined using EIS and obtained via Equation (3):

$$\sigma = \frac{d}{\mathcal{R} \times A} \quad (3)$$

where  $\sigma$  represents the ionic conductivity (S cm<sup>-1</sup> or mS cm<sup>-1</sup>),  $d$  is separator's thickness (cm),  $A$  is the area of the SS electrode (0.8 × 0.8 × π cm<sup>2</sup>), and  $\mathcal{R}$  is the bulk resistance of the separator (Ω).

The battery cycling performance of the separator was investigated using a CR 2025 button-type half-cell. The separator was positioned between the lithium metal anode and the LiFePO<sub>4</sub> cathode (LiFePO<sub>4</sub>/Acetylene black/PVDF = 80/10/10). The cycling performance and C-rate performance measurements were conducted by utilizing the battery cycle tester (BTS 5 V 10 mA, Neware Corporation, Shenzhen, China), with a voltage range of 2.5–4.2 V. The cells' cycling performance was tested at 1 C for 150 charge/discharge cycles. The C-rate Performance was assessed at current densities of 0.1, 0.2, 0.5, 1, 2, 3, and 5 C.

### 3. Results and Discussion

#### 3.1. Morphological Analysis

The SEM images of pure PVA membranes and PVA/CA composite membranes before and after heating treatment are presented in Figures 2 and S1. As can be seen, the pure PVA nanofibrous membrane presents a large number of randomly oriented nanofibers with an average diameter of 170 nm (Figure S1a), and regardless of whether or not they are heat-treated, the nanofibers on these PVA/CA composite membranes (Figure 2a–h)

are also uniformly distributed to form a 3D interweaving network with a thickness of  $\sim 80 \mu\text{m}$  (Figure S1b). Compared to the non-heat-treated PVA/CA membranes (Figure 2a–d), bonding or adhesions between fibers can be clearly seen in the heat-treated PVA/CA-H membranes (Figure 2e–h), and these bonds become more pronounced as the concentration of CA increases. In particular, for the sample of PVA/CA-H8 in Figure 2h, almost all the fibers stick together, and the original fibers lose their fibrous shape, with only a few holes being left.

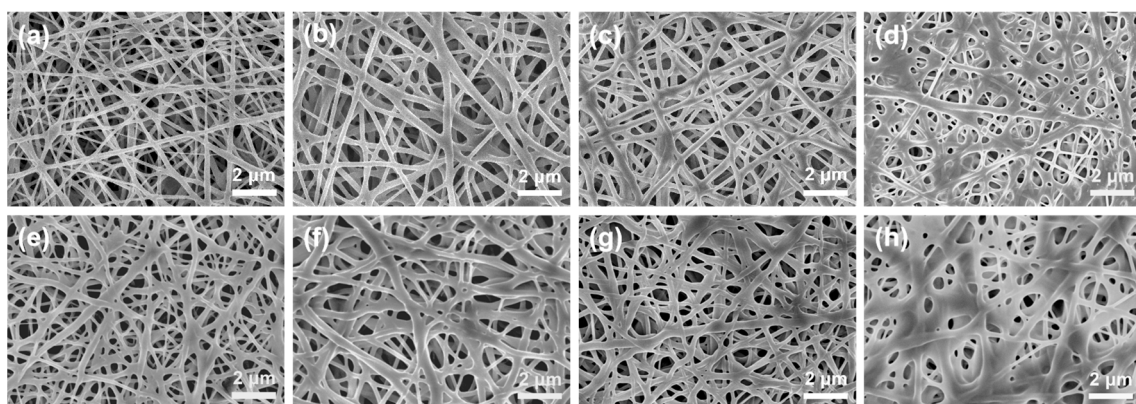


**Figure 2.** SEM images of PVA/CA composite membranes before heating—(a) PVA-CA-2, (b) PVA-CA-4, (c) PVA-CA-6, and (d) PVA-CA-8—and after heating—(e) PVA-CA-H2, (f) PVA-CA-H4, (g) PVA-CA-H6, and (h) PVA-CA-H8.

In order to examine the adhesions produced via the heating process, infrared spectra tests of different nanofibrous membranes are carried out, and the results are shown in Figure 3a. The PVA/CA nanofibrous membranes show characteristic peaks similar to those of pure PVA nanofibrous membranes. Peaks at 3314, 2949, and  $1098 \text{ cm}^{-1}$  correspond to the stretching vibration of O-H, the C-H vibration of alkyl, and the stretching vibration of C-O, respectively [29]. We found a peak at around  $1708 \text{ cm}^{-1}$  in the spectrum of pure PVA, which should be attributed to the fact that the C=O stretching of acetate groups remained in the 1788 type of the PVA raw material [29,30]. Meanwhile, the PVA/CA-H composite membranes treated via heating present an intensified C=O characteristic peak at  $1708 \text{ cm}^{-1}$ , indicating that the chemical crosslinking interaction between the hydroxyl group of PVA and the carboxyl group of CA is induced via the heating treatment. The intensities of the ester group absorption peaks enhance with the increase in citric acid concentration, suggesting that the crosslinking degree between PVA and CA strengthens with the increase in CA content. Moreover, the water-solubility of the crosslinked PVA/CA membrane is checked. As seen in Figure 3b, the PVA/CA membrane without heating treatment dissolves rapidly in water, while the heat-treated PVA/CA-H membrane remains intact, further indicating that the thermal crosslinking reaction between PVA and CA successfully occurred after the heating treatment.

Figure 4a displays the pore size distribution of pure PVA and crosslinked PVA/CA-H composite membranes. It is observed that the pore size of the pure PVA nanofibrous membrane is centrally distributed up to  $0.4 \mu\text{m}$ , and all the PVA/CA-H membranes present smaller pore sizes in the range of  $0.1\text{--}0.4 \mu\text{m}$  due to the blockage of those adhesions. Meanwhile, the pore sizes of the composite membranes decrease gradually with the increase in the citric acid content (Table 1), while the pore size after thermal crosslinking is smaller than that before thermal crosslinking (Figure S2a). However, the pore sizes of these membranes are still larger than those of the commercial PP membrane (20–50 nm) because of the different preparation methods used.

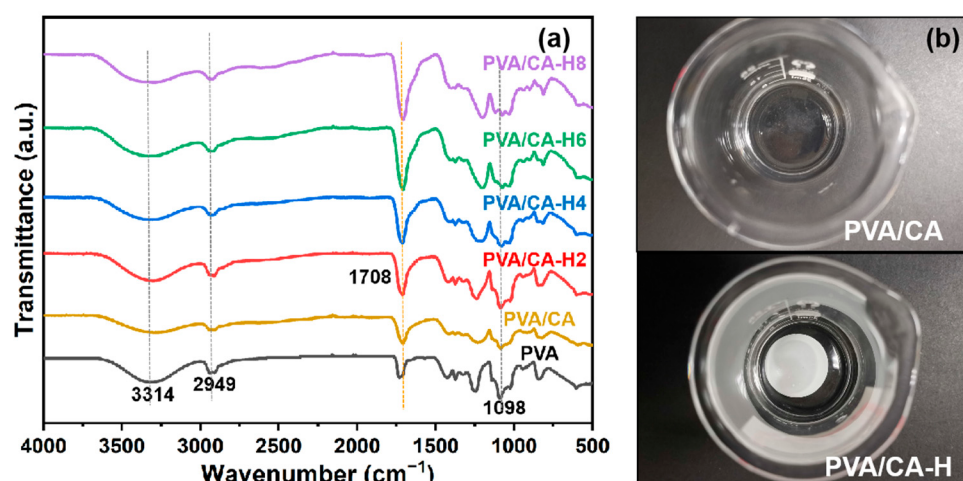


**Figure 3.** (a) FTIR spectra of different membranes; (b) optical pictures of PVA/CA membrane and PVA/CA-H membrane immersed in water.

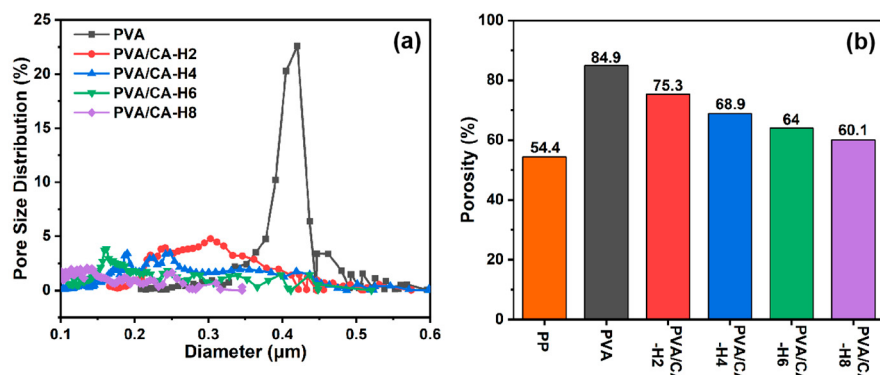


**Figure 4.** (a) Pore size distribution of PVA and its composite membranes, and (b) porosity of commercial PP separator and different PVA composite membranes.

**Table 1.** Basic parameters of PVA and its crosslinked PVA/CA-H composite separators.

Sample	Thickness (μm)	Density (g/cm <sup>3</sup> )	Mean Pore Size (μm)	Porosity (%)	Tensile Strength (MPa)	Elongation at Break (%)	Electrolyte Uptake (%)
PVA	70 ± 5	0.29	0.4181	84.9	7.4	70.8	374.3
PVA/CA-H2	79 ± 4	0.55	0.2742	75.3	12.9	65.9	174.3
PVA/CA-H4	80 ± 5	0.65	0.2251	68.9	13.2	57.8	158.1
PVA/CA-H6	81 ± 4	0.71	0.1727	64.0	13.7	47.3	118.2
PVA/CA-H8	82 ± 3	0.77	0.1255	60.0	13.6	31.9	84.5

It is well known that nanofibrous membranes subject to electrospinning usually have high porosity because of the 3D network formed via the random arrangement of nanofibers, and, in this study, the effect of crosslinking on the porosity is examined. As shown in Figure 4b, the porosity of the pure PVA membrane is higher than 80%, while the porosity of the PVA/CA-H membrane decreases gradually with the increase in the CA concentration, and it is lower than that before heating (Figure S2b) due to the thermal crosslinking of PVA and CA, which makes the membrane less porous. Although the PVA/CA-H membrane's porosity decreases to a minimum of 60.1%, it is still superior to that of the commercial PP membrane (Celgard 2400, 54.4%). Higher porosity allows greater electrolyte uptake in the separator, and it is beneficial in promoting rapid ion transport and giving higher ionic conductivity, which will be discussed later in this paper.

### 3.2. Mechanical Properties

An ideal separator should have excellent mechanical strength in terms of tensile and puncture to protect against deformation induced during assembly and resist the penetration of electrode burrs and lithium dendrites generated during cycling. Figure 5a depicts the stress–strain curves of pure PVA and crosslinked PVA/CA-H composite nanofibrous membranes. For comparison, the stress–strain curves of the PVA/CA composite membrane before thermal crosslinking are presented in Figure S3a. As can be seen, the uncrosslinked PVA/CA membranes exhibit higher tensile strength and elongation at break than the pure PVA, increasing by 28.4% and 65.4%, respectively (Figure S3a). The remarkable increase in elongation at break can be ascribed to the addition of CA, increasing the interstitial volume of the material and the mobility of the polymer macromolecules [31]. Moreover, once the PVA and CA are crosslinked, the tensile strength of the composite membrane is further enhanced from 7.4 MPa to 13.7 MPa with the increase in the CA content, but its elongation at break decreases from 70.8% to 31.9% (Table 1). The enhancement of tensile strength can be attributed to the chemical crosslinking reactions and hydrogen bonding interactions; however, these interactions simultaneously restrict the movement of the molecular chain segments, thus leading to a decline in elongation at break [32,33]. Therefore, citric acid crosslinking can appreciably enhance the tensile strength of the pure PVA membrane and make it compatible with that of the commercial PP membrane (12.1 MPa) in the transverse direction, even though the longitudinal tensile strength of the PVA/CA-H membrane is much lower than that of the commercial PP membrane (122.8 MPa) [34].

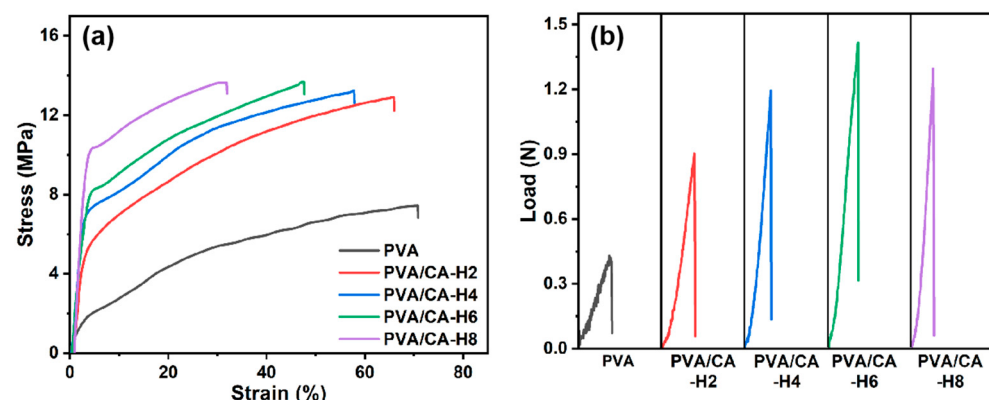


**Figure 5.** (a) Stress–strain curves and (b) puncture load–displacement curves for PVA and PVA/CA-H composite separators.

The puncture performances of different membranes are demonstrated in Figure 5b. Compared to the pure PVA nanofibrous membrane, the puncture resistance of the PVA/CA nanofibrous membrane before thermal crosslinking is improved, with the load increasing from 0.43 N to 0.73 N (Figure S3b). After thermal crosslinking, the load of PVA/CA-H composite membrane is increased to 1.42 N, demonstrating the great increase in the puncture resistance induced via thermal crosslinking. Moreover, with the increase in the CA content, it shows a trend of strengthening and then slightly decreasing, which is the same as the trend of tensile strength. Based on the analysis of tensile and puncture performance, therefore, the mechanical properties of PVA nanofibrous membrane are significantly improved, which should be ascribed to the increased bonding of fibers after thermal crosslinking, providing greater resistance to deformation during stretching and puncturing.

### 3.3. Thermal Properties

The TG and DTG profiles of the pure PVA and different PVA/CA-H nanofibrous membranes are shown in Figures 6a and S4 with regard to the investigation of their thermal stability. As shown, the first weight loss temperature of all the samples is below 100 °C owing to the evaporation of water. As the temperature increases, the PVA membrane

exhibits significant weight loss from 260 °C, with a maximum rate of weight loss detected at 330 °C (Figure S4). When CA is added to PVA, all PVA/CA-H separators show two major regions of weight loss: one from 180 °C to 260 °C for the decomposition of CA, and the other from 260 °C to 510 °C for the decomposition of PVA. In particular, the weight loss from 260 °C to 410 °C is due to the thermal decomposition of the PVA side chains, with the products consisting of small particles of carbon and hydrocarbons, while the degradation process from 410 °C to 510 °C is related to the disintegration of the PVA main chains [35,36]. Meanwhile, the thermal dimensional stability test is performed by gradually heating the separators. As shown in Figure 6b, the PP separator shrinks strongly at 120 °C and melts at 180 °C, while the PVA separator shrinks slightly at 120 °C and severely at 180 °C. In comparison, the thermally crosslinked PVA/CA-H separators can keep their shape intact at 180 °C, suggesting that their thermal dimensional stability was improved via the crosslinking modification.

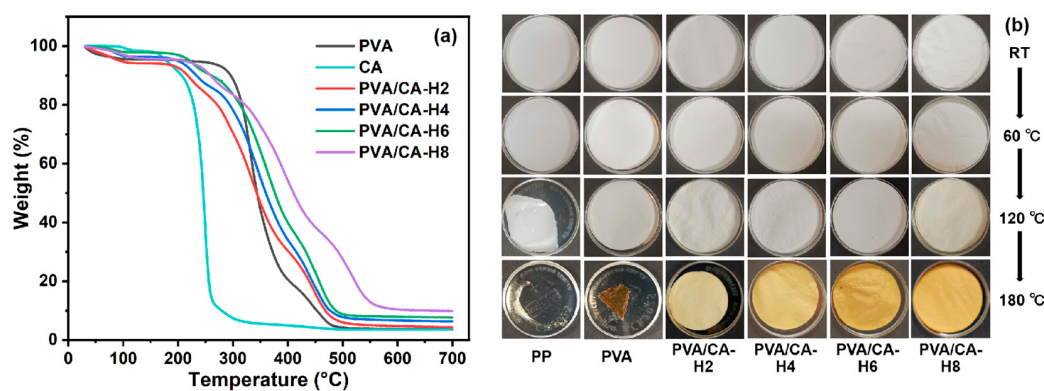


**Figure 6.** (a) The TG curves of CA and different separators in heating scan, and (b) the optical photographs of separators treated for 1 h at different temperatures.

### 3.4. Electrolyte Wettability

The electrolyte wettability and electrolyte uptake of the separator are critical to the performance of LIBs. The excellent electrolyte wettability of the separator not only improves the rate of ion transport but also enables faster battery assembly, which, in turn, enhances the cycle stability and multiplier performances of LIBs. The variation in the electrolyte contact angle with time for various separators is demonstrated in Figure 7a. It remains unspread after 10 s, when the electrolyte drops onto the surface of the PP separator because the PP separator has a hydrophobic surface and low surface energy, resulting in poor wettability with the electrolyte. The PVA membrane can be quickly wetted by the electrolyte with only 1.2 s of complete wetting due to its rich hydroxyl group with a high degree of pro-electrolyte behavior. And the PVA/CA membranes still have excellent electrolyte wetting properties before thermal crosslinking (Figure S5a). After thermal crosslinking, the complete wettability of the PVA/CA-H membranes becomes longer, and the wettability deteriorates with increasing CA. It is attributed to the fact that the excessive addition of CA leads to a decrease in the porosity of the PVA/CA separators, which hinders the infiltration of the electrolyte. Nevertheless, the PVA/CA-H composite separators still have better electrolyte wettability than the commercial PP separator.

The electrolyte absorption capacity of the separators is shown in Figure 7b, in which the changing trend for the electrolyte uptake of each separator is consistent with that of the porosity. The PVA membrane has a high uptake value of 374.3% thanks to its excellent porosity and superior wettability. With the increase in CA, the electrolyte uptake of the PVA/CA-H separators decreases, and it is lower than that before thermal crosslinking (Figure S5b), which is attributed to the decrease in the porosity of the separator caused by the addition of CA. In general, the PVA/CA-H separators still exhibit good electrolyte uptake performance (>84.5%) compared to the PP separator (79.7%), which is favorable to

increasing the ionic conductivity and improving the charging and discharging performance of the batteries.

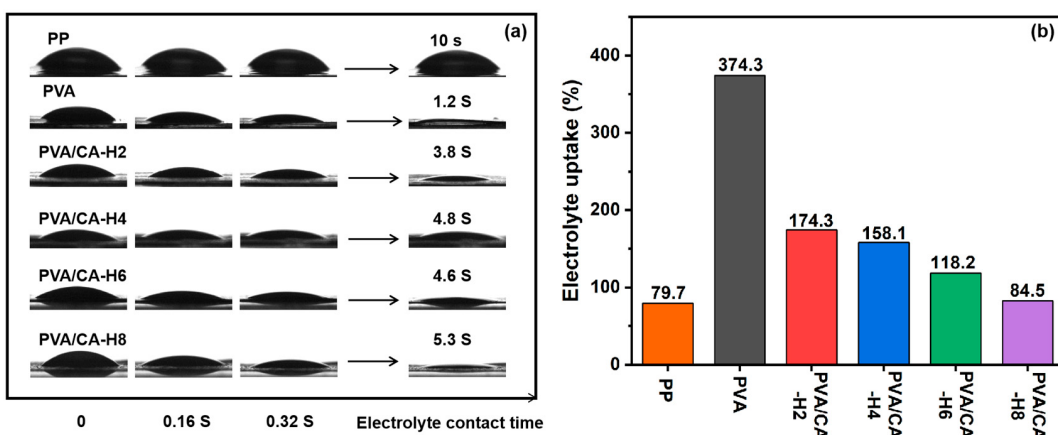


**Figure 7.** (a) Electrolyte contact angle with changes over time, and (b) the electrolyte uptake of different separators.

### 3.5. Electrochemical Properties

In the previous section, we comprehensively evaluated the porosity and mechanical, thermal, and electrolyte wetting properties of various separators. The PVA/CA-H4 separator is selected for the next step of electrochemical and battery performance testing because of its high porosity, good mechanical and thermal properties, and excellent wettability.

Figure 8a shows the Nyquist plots of cells assembled with different separators, where the bulk resistance and ionic conductivity of the separators can be determined. The ionic conductivity of the PVA/CA-H4 separator is calculated to be 1.63 mS/cm, which is significantly higher than that of the commercial PP separator (0.59 mS/cm) and the pure PVA separator (1.27 mS/cm). One of the reasons for this result is the good porosity and excellent electrolyte wettability of the PVA/CA-H4 separator, which facilitates the efficient transport of Li-ions during the charging and discharging of the battery.

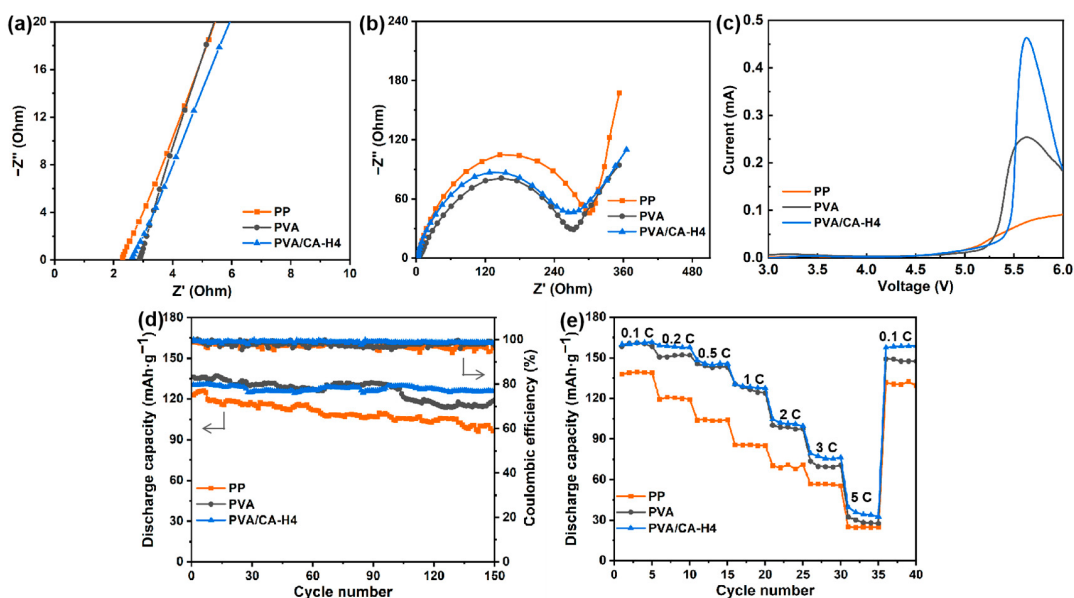


**Figure 8.** (a) Nyquist plots for SS/separator/SS batteries, (b) Nyquist plots for LiFePO<sub>4</sub>/separator/Li batteries, (c) LSV curves for Li/separator/SS batteries from 3 to 6 V, and (d) cycling performance and (e) rate performance for LiFePO<sub>4</sub>/separator/Li batteries assembled using the commercial PP separator and PVA and the crosslinked PVA/CA-H4 separators.

The interfacial resistance of each separator is shown in Figure 8b, where the semicircle radius in the impedance spectrum stands for the electrode–electrolyte interfacial resistance ( $R_{in}$ ). The  $R_{in}$  of commercial PP, PVA, and PVA/CA-H4 separators are 327.8, 290.4, and 285.2  $\Omega$ , respectively. The lower  $R_{in}$  of the PVA/CA-H4 separator compared to the PP separator may be attributed to its higher porosity and better electrolyte wettability. As a result, the PVA/CA-H4 separator has better interfacial stability, which promotes the transport of ions at the electrode–electrolyte interface, leading to decreased overall cell resistance and improved cell performance.

As shown in Figure 8c, the electrochemical stability window was evaluated by recording the LSV curves of the separators from 3 V to 6 V. As the current grows at an exponential rate, the corresponding voltage is the limit voltage of electrochemical oxidation. It is demonstrated that the anodic stability values of PVA and PVA/CA-H4 separators are as high as 4.9 V and 5.0 V versus  $\text{Li}^+/\text{Li}$ , respectively, higher than that of the commercial PP separator (4.7 V). The ideal electrochemical stability of the PVA/CA-H4 composite separator can be attributed to its good swelling ability, and its excellent porous structure and good porosity can trap more electrolytes, as well as delay the electrolytes' decomposition.

### 3.6. Battery Performance

The cycling and rate performances of cells with the PVA/CA-H4 separator are evaluated by using cells with the commercial PP separator and pure PVA separator as the control groups. Figure 8d shows the cycle performance and Coulombic efficiency of cells assembled using different separators at 1 C. It can be observed that the PVA/CA-H4 separator has an initial discharge-specific capacity of 131  $\text{mAh}\cdot\text{g}^{-1}$ , which is higher than that of the commercial PP separator (123  $\text{mAh}\cdot\text{g}^{-1}$ ) but lower than that of the pure PVA separator (136  $\text{mAh}\cdot\text{g}^{-1}$ ). In addition, after 150 cycles at 1 C, the cell assembled with the PVA/CA-H4 separator shows stable a specific capacity, with a capacity retention of 96.3% and a Coulombic efficiency of 98.8%, while the PP separator exhibits a capacity retention of 78.4% and a Coulombic efficiency of about 96.8%. It demonstrates that the batteries assembled via the PVA/CA-H4 separator lose less power during charging and discharging and have good battery cycling performance, which increases the performance and lifetime of the batteries.

The rate performance of each separator at 0.1 C to 5 C is demonstrated in Figure 8e. The discharge-specific capacities of the batteries with commercial PP and PVA separators are 138 and 158  $\text{mAh}\cdot\text{g}^{-1}$  at 0.1 C, respectively, decreasing to 24 and 27  $\text{mAh}\cdot\text{g}^{-1}$  at 5 C. In comparison, the cell with PVA/CA-H4 separator exhibits an initial capacity of 160  $\text{mAh}\cdot\text{g}^{-1}$  at 0.1 C and decreases to 33  $\text{mAh}\cdot\text{g}^{-1}$  at 5 C. The discharge-specific capacity is recovered when the rate returns to 0.1 C, demonstrating the excellent reversibility of the cell. The improved rate performance of the PVA/CA-H4 separator can be attributed to its good pore size distribution and fast Li-ion conductivity.

## 4. Conclusions

In summary, we successfully prepared the PVA/CA-H composite separators using the crosslinking technique and investigated their porous structure and wettability, thermal and mechanical properties, and electrochemical and battery performance. Although the PVA/CA-H composite separator showed reduced pore size and decreased porosity due to crosslinking compared to the pure PVA separator, it exhibited higher mechanical strength and better thermal stability. Moreover, it still possessed a rich porous structure and good electrolyte wettability, thus demonstrating high ionic conductivity and desirable electrochemical performance. Thus, the cell equipped with the PVA/CA-H composite separator showed excellent battery performance, having a capacity retention rate of 96.3% after 150 cycles at 1 C. Consequently, the prepared PVA/CA-H composite separator could provide a promising alternative for the development of high-safety and high-performance LIBs.

**Supplementary Materials:** The following supporting information can be downloaded via this link: <https://www.mdpi.com/article/10.3390/batteries9110556/s1>, Figure S1: SEM surface images of (a) PVA and (b) SEM cross-section image of PVA/CA-H4; Figure S2: (a) Pore size distribution and (b) porosity of different membranes before thermal treatment; Figure S3: (a) Stress-strain curves and (b) puncture load-displacement curves for different PVA/CA composite membranes before thermal treatment; Figure S4: DTG curves of CA and different separators in heating scan; Figure S5: (a) Electrolyte contact angle changing with time and (b) the electrolyte uptake for different PVA/CA composite membranes before thermal treatment.

**Author Contributions:** Validation, Formal analysis, Investigation, Writing—original draft, S.C.; Validation, Investigation, Y.L.; Data curation, J.W.; Data curation, H.C.; Conceptualization, Writing—review & editing, Supervision, Z.W.; Supervision, Y.Z. All authors have read and agreed to the published version of the manuscript.

**Funding:** This work was financially supported by the Natural Science Foundation of the Jiangsu Higher Education Institutions of China (22KJA480004), the Key Laboratory of Flame Retardancy Finishing of Textile Materials, CNTAC (Q811580421), and the Qing Lan Project.

**Data Availability Statement:** The data presented in this study are available on request from the corresponding author. The data are not publicly available due to privacy.

**Conflicts of Interest:** The authors declare that they have no known competing financial interests or personal relationships that could have appeared to influence the work reported in this paper.

## References

1. Costa, C.M.; Lee, Y.-H.; Kim, J.-H.; Lee, S.-Y.; Lanceros-Méndez, S. Recent advances on separator membranes for lithium-ion battery applications: From porous membranes to solid electrolytes. *Energy Storage Mater.* **2019**, *22*, 346–375. [[CrossRef](#)]
2. Yuan, M.; Liu, K. Rational design on separators and liquid electrolytes for safer lithium-ion batteries. *J. Energy Chem.* **2020**, *43*, 58–70. [[CrossRef](#)]
3. Wang, F.; Ke, X.; Shen, K.; Zhu, L.; Yuan, C. A Critical Review on Materials and Fabrications of Thermally Stable Separators for Lithium-Ion Batteries. *Adv. Mater. Technol.* **2021**, *7*, 2100772. [[CrossRef](#)]
4. Ahn, Y.K.; Kwon, Y.K.; Kim, K.J. Surface-modified polyethylene separator with hydrophilic property for enhancing the electrochemical performance of lithium-ion battery. *Int. J. Energy Res.* **2020**, *44*, 6651–6659. [[CrossRef](#)]
5. Kim, K.J.; Kwon, Y.K.; Yim, T.; Choi, W. Functional separator with lower resistance toward lithium ion transport for enhancing the electrochemical performance of lithium ion batteries. *J. Ind. Eng. Chem.* **2019**, *71*, 228–233. [[CrossRef](#)]
6. Liu, Y.; Zhang, Z.; Du, X.; Wang, Y.; Guo, X.; Yu, M.; Liu, B.; Hu, W.; Shen, L.; Lu, Y.; et al. Poly(ether ether ketone) Conferred Polyolefin Separators with High Dimensional Thermal Stability for Lithium-Ion Batteries. *ACS Appl. Mater. Interfaces* **2023**, *15*, 37354–37360. [[CrossRef](#)]
7. Hao, W.Q.; Kong, D.C.; Xie, J.M.; Chen, Y.P.; Ding, J.; Wang, F.H.; Xu, T.T. Self-Polymerized Dopamine Nanoparticles Modified Separators for Improving Electrochemical Performance and Enhancing Mechanical Strength of Lithium-Ion Batteries. *Polymers* **2020**, *12*, 648. [[CrossRef](#)]
8. Zhu, M.; Wang, Q.; Zhou, H.H.; Qi, L.M. Binder-Free TiO<sub>2</sub>-Coated Polypropylene Separators for Advanced Lithium-Ion Batteries. *Energy Technol.* **2020**, *8*, 2000228. [[CrossRef](#)]
9. Zhang, H.; Sheng, L.; Bai, Y.Z.; Song, S.J.; Liu, G.J.; Xue, H.R.; Wang, T.; Huang, X.L.; He, J.P. Amino-Functionalized Al<sub>2</sub>O<sub>3</sub> Particles Coating Separator with Excellent Lithium-Ion Transport Properties for High-Power Density Lithium-Ion Batteries. *Adv. Eng. Mater.* **2020**, *22*, 1901545. [[CrossRef](#)]
10. Gao, X.; Sheng, L.; Xie, X.; Yang, L.; Bai, Y.; Dong, H.; Liu, G.; Wang, T.; Huang, X.; He, J. Morphology optimizing of polyvinylidene fluoride (PVDF) nanofiber separator for safe lithium-ion battery. *J. Appl. Polym. Sci.* **2022**, *139*, 52154. [[CrossRef](#)]
11. Luiso, S.; Henry, J.J.; Pourdeyhimi, B.; Fedkiw, P.S. Meltsblown Polyvinylidene Difluoride as a Li-Ion Battery Separator. *ACS Appl. Polym. Mater.* **2021**, *3*, 3038–3048. [[CrossRef](#)]
12. Dong, T.; Arifeen, W.U.; Choi, J.; Yoo, K.; Ko, T. Surface-modified electrospun polyacrylonitrile nano-membrane for a lithium-ion battery separator based on phase separation mechanism. *Chem. Eng. J.* **2020**, *398*, 125646. [[CrossRef](#)]
13. Sabetzadeh, N.; Gharehaghaji, A.A.; Javanbakht, M. Porous PAN micro/nanofiber membranes with potential application as Lithium-ion battery separators: Physical, morphological and thermal properties. *J. Polym. Res.* **2019**, *26*, 20. [[CrossRef](#)]
14. Yang, W.; Minhao, G.; Hui, F.; Zhenzhong, W.; Yizhe, Z.; Guojie, C.; Suli, C.; Longsheng, Z.; Tianxi, L. Thermotolerant separator of cross-linked polyimide fibers with narrowed pore size for lithium-ion batteries. *J. Membr. Sci.* **2022**, *662*, 121004.
15. Sun, G.; Jiang, S.; Feng, X.; Shi, X.; Zhang, X.; Li, T.; Chen, N.; Hou, L.; Qi, S.; Wu, D. Ultra-robust polyimide nanofiber separators with shutdown function for advanced lithium-ion batteries. *J. Membr. Sci.* **2021**, *645*, 120208. [[CrossRef](#)]
16. Cheng, C.; Yang, R.; Wang, Y.; Fu, D.; Sheng, J.; Guo, X. A bacterial cellulose-based separator with tunable pore size for lithium-ion batteries. *Carbohydr. Polym.* **2023**, *304*, 120489. [[CrossRef](#)]

17. Wang, Y.; Liu, X.; Sheng, J.; Zhu, H.; Yang, R. Nanoporous Regenerated Cellulose Separator for High-Performance Lithium Ion Batteries Prepared by Nonsolvent-Induced Phase Separation. *ACS Sustain. Chem. Eng.* **2021**, *9*, 14756–14765. [[CrossRef](#)]
18. Dai, X.; Zhang, X.; Wen, J.; Wang, C.; Ma, X.; Yang, Y.; Huang, G.; Ye, H.-M.; Xu, S. Research progress on high-temperature resistant polymer separators for lithium-ion batteries. *Energy Storage Mater.* **2022**, *51*, 638–659. [[CrossRef](#)]
19. Ding, L.; Yan, N.; Zhang, S.; Xu, R.; Wu, T.; Yang, F.; Cao, Y.; Xiang, M. Separator impregnated with polyvinyl alcohol to simultaneously improve electrochemical performances and compression resistance. *Electrochim. Acta* **2022**, *403*, 139568. [[CrossRef](#)]
20. Chen, Y.; Zhou, G.; Zong, W.; Ouyang, Y.; Chen, K.; Lv, Y.; Miao, Y.-E.; Liu, T. Porous polymer composite separators with three-dimensional ion-selective nanochannels for high-performance Li–S batteries. *Compos. Commun.* **2021**, *25*, 100679. [[CrossRef](#)]
21. Xie, Y.; Pan, Y.; Cai, P. Novel PVA-Based Porous Separators Prepared via Freeze-Drying for Enhancing Performance of Lithium-Ion Batteries. *Ind. Eng. Chem. Res.* **2020**, *59*, 15242–15254. [[CrossRef](#)]
22. Chen, P.; Xing, W.; Yuting, F.; Zhenzhen, W.; Yan, Z.  $\text{WO}_3$ -composited polyimide nanofibrous separator with superior mechanical properties and high capacity for lithium-ion batteries. *J. Mater. Sci.* **2023**, *58*, 10686–10698.
23. Xiao, W.; Song, J.; Huang, L.; Yang, Z.; Qiao, Q. PVA– $\text{ZrO}_2$  multilayer composite separator with enhanced electrolyte property and mechanical strength for lithium-ion batteries. *Ceram. Int.* **2020**, *46*, 29212–29221. [[CrossRef](#)]
24. Zhang, S.; Wang, X.; Liang, J.; Gu, J.; Feng, X.; Xu, C. Preparation of High Performance Lithium-Ion Battery Separators by Double-Needle Electrospinning. *ChemistrySelect* **2022**, *7*, e202203407. [[CrossRef](#)]
25. Dastidar, T.G.; Netravali, A.N. ‘Green’ crosslinking of native starches with malonic acid and their properties. *Carbohydr. Polym.* **2012**, *90*, 1620–1628. [[CrossRef](#)]
26. Khodaverdi, F.; Vaziri, A.; Javanbakht, M.; Jahanfar, M. Improvement of PAN separator properties using PVA/malonic acid by electrospinning in lithium ion-batteries. *J. Appl. Polym. Sci.* **2020**, *138*, 50088. [[CrossRef](#)]
27. Gong, Z.; Zheng, S.; Zhang, J.; Duan, Y.; Luo, Z.; Cai, F.; Yuan, Z. Cross-Linked PVA/HNT Composite Separator Enables Stable Lithium-Organic Batteries under Elevated Temperature. *ACS Appl. Mater. Interfaces* **2022**, *14*, 11474–11482. [[CrossRef](#)]
28. Jeong, S.; Oh, S.-G. Antiacne Effects of PVA/ZnO Composite Nanofibers Crosslinked by Citric Acid for Facial Sheet Masks. *Int. J. Polym. Sci.* **2022**, *2022*, 4694921. [[CrossRef](#)]
29. Ge, J.C.; Wu, G.; Yoon, S.K.; Kim, M.S.; Choi, N.J. Study on the Preparation and Lipophilic Properties of Polyvinyl Alcohol (PVA) Nanofiber Membranes via Green Electrospinning. *Nanomaterials* **2021**, *11*, 2514. [[CrossRef](#)]
30. Alhosseini, S.N.; Moztarzadeh, F.; Mozafari, M.; Asgari, S.; Dodel, M.; Samadikuchaksaraei, A.; Kargozar, S.; Jalali, N. Synthesis and characterization of electrospun polyvinyl alcohol nanofibrous scaffolds modified by blending with chitosan for neural tissue engineering. *Int. J. Nanomed.* **2012**, *7*, 25–34.
31. Wang, S.; Ren, J.; Li, W.; Sun, R.; Liu, S. Properties of polyvinyl alcohol/xylan composite films with citric acid. *Carbohydr. Polym.* **2014**, *103*, 94–99. [[CrossRef](#)]
32. Jiang, S.; Qiao, C.; Liu, R.; Liu, Q.; Xu, J.; Yao, J. Structure and properties of citric acid cross-linked chitosan/poly(vinyl alcohol) composite films for food packaging applications. *Carbohydr. Polym.* **2023**, *312*, 120842. [[CrossRef](#)]
33. Wen, L.; Liang, Y.; Lin, Z.; Xie, D.; Zheng, Z.; Xu, C.; Lin, B. Design of multifunctional food packaging films based on carboxymethyl chitosan/polyvinyl alcohol crosslinked network by using citric acid as crosslinker. *Polymer* **2021**, *230*, 124048. [[CrossRef](#)]
34. Zhang, K.; Chen, H.; Huang, H.; Wei, Z.; Zhao, Y. Water-soluble ammonium polyphosphate synchronously enables mechanically robust and flame-retardant cellulose composite separator for high safety lithium batteries. *J. Power Sources* **2023**, *558*, 232627. [[CrossRef](#)]
35. Yu, D.; Feng, Y.Y.; Xu, J.X.; Kong, B.H.; Liu, Q.; Wang, H. Fabrication, characterization, and antibacterial properties of citric acid crosslinked PVA electrospun microfibre mats for active food packaging. *Packag. Technol. Sci.* **2021**, *34*, 361–370. [[CrossRef](#)]
36. Qin, X.; Dou, G.; Jiang, G.; Zhang, S. Characterization of poly (vinyl alcohol) nanofiber mats cross-linked with glutaraldehyde. *J. Ind. Text.* **2012**, *43*, 34–44. [[CrossRef](#)]

**Disclaimer/Publisher’s Note:** The statements, opinions and data contained in all publications are solely those of the individual author(s) and contributor(s) and not of MDPI and/or the editor(s). MDPI and/or the editor(s) disclaim responsibility for any injury to people or property resulting from any ideas, methods, instructions or products referred to in the content.